New Journal of Physics
The open access journal for physics

# Eliminating spatial distortions in Anger-type gamma cameras

**Michael Leitner**[1], **Hubert Ceeh and Josef-Andreas Weber**
Forschungs-Neutronenquelle Heinz Maier-Leibnitz (FRM II),
Technische Universität München, 85747 Garching, Germany
E-mail: michael.leitner@frm2.tum.de

*New Journal of Physics* **14** (2012) 123014 (13pp)
Received 26 October 2012
Published 10 December 2012
Online at http://www.njp.org/
doi:10.1088/1367-2630/14/12/123014

**Abstract.** A procedure to quantify and correct the spatial distortions inherent to Anger-type gamma cameras is presented. It consists in imaging a pattern of regularly spaced holes, assigning to each pair of lattice indices the actual position on the detector and generating a look-up matrix describing the inverse mapping. This allows one to correct the position of the distinct events either during or after the measurement with minimal computational effort. The corrected spectrum is indistinguishable from a spectrum taken with an ideal detector in a statistical sense. The effect of the increased resolution on measurements of angular correlation of positron annihilation radiation is demonstrated. The presented scheme is applicable for all types of area detectors.

[1] Author to whom any correspondence should be addressed.

## Contents



## 1. Introduction

Two-dimensional position-sensitive gamma detectors of Anger type (Anger 1958) are standard tools in diverse fields of physics (West *et al* 1981, Parmar *et al* 1997, Schultz *et al* 2006, Engels *et al* 2009, Coates *et al* 2010) and probably even more widely deployed in nuclear medicine (Zanzonico and Heller 2007). In a camera of this type the incident gamma photon generates a localized flash of light in the scintillation crystal, which is detected by an array of photo-multiplier tubes. Information on the position of the event is obtained by computing the average of the position of the responding photo-multipliers, weighted by their respective responses. It is clear that a naive implementation of this principle would give large distortions in the position assignment due to the fact that the detector response varies nonlinearly with the distance from the scintillation event to the photo-multiplier centre. Also the sum signal (used for energy discrimination) would be much higher for a photon absorbed directly before a photo-multiplier than for a photon of the same energy detected in the area between two photo-multipliers.

The state of the art is therefore to use weighting factors for the position determination (and for the sum signal) that depend nonlinearly on the photo-multiplier response (Short 1984). This is normally done by an analogue or digital logic integrated in the detector. Specifically for the position determination it is evident, however, that even if the nonlinear weighting functions are chosen ideally, residual distortions will remain, as general two-dimensional vector fields (the distortions) cannot be described (and inverted) by a one-dimensional nonlinear correction function. Additionally, spatial inhomogeneities of the crystal or detector response and temporal drift of the components will further degrade the performance.

The effect of distortions is twofold: on the one hand, features of the imaged pattern are displaced from their ideal positions (distorted in the narrow sense of the word); on the other hand, a spatially varying displacement also leads to modulations in the apparent brightness of an ideally flat image, as events corresponding to a certain detector area are actually spread over smaller or larger areas (Wicks and Blau 1979). The latter is the primary detrimental effect

in medical applications like scintigraphy, where the intensity modulations would ideally be given only by the varying enrichment with the radioactive tracer, on which the diagnosis relies. In contrast, small displacements are inconsequential, as the spatial resolution for this type of examination is poor in any case. For other applications, especially when used as detectors for physical experiments, the situation can be different: here, very often, the position of the events is the main experimental goal.

A number of investigations of the spatial distortions and their effects, as well as proposals to correct for these distortions, have been put forward: Wicks and Blau (1979) showed that the major part of the flood field nonuniformity is due to spatial distortions as opposed to variations in sensitivity, and early solutions using a dedicated micro-processor were proposed and presented by Knoll and Schrader (1982) and Muehllehner *et al* (1980). With the availability of personal computers the possibility to treat these issues in software has become attractive, which has been demonstrated by Stanton *et al* (1992) and extensively discussed by Hammersley *et al* (1994). All these approaches agree in determining the distortions by imaging a mask of regularly spaced lines or holes. In contrast, Johnson *et al* (1996) and Barendt *et al* (2007) propose to directly determine the distortions as the minimal correction that yields an ideal flat image from a measured flood field. Most of these proposals have been written from the viewpoint of medical physics and therefore put the main focus on the achieved uniformity of flood fields.

Here we present a solution to the spatial distortion problem where our main aim is the correct assignment of the position of the detected events, and we evaluate its performance from the viewpoint of angular correlation of positron annihilation radiation (ACPAR) (West 1995). This method consists in detecting the deviation from anti-collinear propagation directions of pairs of annihilation quanta, i.e. essentially summing the positions of coincident events on opposite detectors. Our approach uses commercially available perforated sheet metal as a mask and distortion detection and correction algorithms implemented in software. It can therefore be used to significantly improve the performance of existing detector systems without much effort. Even though we discuss the nature of the distortions and the achieved performance for the special case of Anger cameras, our approach is valid for all types of position-sensitive detectors that display spatial distortions of any kind.

## 2. Distortion detection and inversion

### *2.1. Detector specifications*

We demonstrate our case with the newly installed two-dimensional ACPAR spectrometer installed in Munich (Ceeh *et al* 2012). It employs Anger cameras manufactured by AuRa Scientific that are optimized for ACPAR experiments, i.e. they have no collimator. They consist of a regular hexagonal array of 61 photo-multiplier tubes with 6.8 cm detector separation optically coupled to a 1.05 cm thick thallium-doped NaI crystal. The field of view is defined by a circular lead aperture of 41.5 cm diameter. We use a sample–detector distance of 8.25 m. Energy discrimination and position determination are done by an analogue arithmetic implemented as a resistor network. The signals are read out with 11 bit resolution.

Due to the nature of Anger cameras, there is no inherent position discretization into pixels. Therefore there are a number of parameters to be set manually, which include the energy amplification and the offset and gain of the two spatial dimensions, respectively. Naturally, these

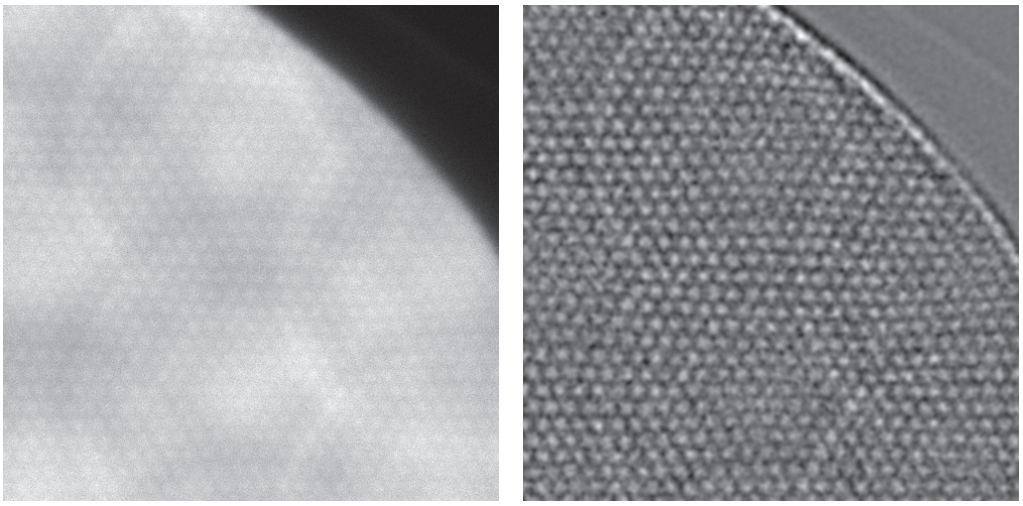

**Figure 1.** Detail of the image of the hole pattern on the detector before (left) and after enhancement (right) as discussed in the text.

are chosen so that the field of view fits comfortably into the acceptance range of the analogue-to-digital converter. However, it is clear that this aspect necessitates a calibration of the camera in some way so as to be able to interpret the position information quantitatively.

Additionally, the response of each of the 61 photo-multipliers can be independently linearly amplified. We calibrated these amplification factors by the edge of the photopeak resulting from positioning a radioactive source directly in front of the respective photo-multiplier tube. Consequently, the intrinsic performance of the detectors is at their optimum, and residual distortions and flood field inhomogeneities have to be due to the inherent principle of Anger cameras (the discrete arrangement of the photo-multiplier tubes), or to deviations in the characteristics of the photo-multipliers or the nonlinear amplification circuits of the respective photo-multiplier signals.

### *2.2. Calibration pattern images*

In order to determine the distortion vector field, the response of the camera to photons impinging at known positions has to be recorded. This can be done by moving a well-collimated source in steps over the detector (Engeland 2001). However, it is much easier and faster to illuminate a known pattern by a distant point source. The optimal pattern has been discussed in detail by Hammersley *et al* (1994), and custom-mode hole and line patterns have been used by, e.g., Muehllehner *et al* (1980) and Stanton *et al* (1992). On the other hand, perforated sheet metal, which is a standard raw material and available in different arrangements and spacings of holes, is equally suited to this task. We used an 8 mm stack of steel sheets with a hexagonal arrangement of round holes of 3 mm diameter and 5 mm spacing (DIN 24041 Rv 3-5).

A detail of the resulting image is given in the left panel of figure 1. Although the hexagonal pattern can be discerned clearly, it is affected by counting noise (at about 450 counts per channel) and is rather weak, corresponding to a modulation with an amplitude of about 2.5%. This is partly due to the fact that our 8 mm thick mask has a transmission of about 59% for 511 keV photons (we refrained from using a thicker mask due to weight issues). More important,

however, is the fact that the width of the point spread function, i.e. the inherent statistical noise due to the physical process of detection, is not much less than the hole diameter in our case, leading to an overlap of the signal from neighbouring holes. Hammersley *et al* (1994) give as a rule of thumb that the hole diameter should be at least six times the width of the point spread function for the spots to be clearly separated. In our opinion, such a coarse pattern is not advisable due to the concomitant loss of information. Rather, we enhance our pattern in software.

We proceed as follows: we set a threshold to distinguish between the illuminated regions and those behind the lead aperture defining the field of view. We then define an auxiliary two-dimensional data array that has entries equal to zero in the illuminated regions and entries equal to the mean of the illuminated regions on the outside. We then convolve this auxiliary array with a Gaussian smoothing kernel and add it to the original data. This serves to diminish the edge effects. As a second step, we convolve the array by the difference of two normalized Gaussian kernels with widths that differ by a factor of 2. This effectively constitutes a band-pass filter with smooth response characteristic. The result is given in the right panel of figure 1, which shows that after such an enhancement the maxima are distinctly visible.

### *2.3. Determining the distortion vector field*

Of course it is not practical to map out the positions of the mask holes on the detector by hand. Published solutions (Stanton *et al* 1992, Hammersley *et al* 1994) agree in first assigning the distorted positions of the mask holes exactly to the peaks and afterwards fitting a smooth function to these positions, taking care of the unavoidable statistical errors in determining the positions. This approach is only viable when the peaks are clearly separated and the variation between maxima and minima is high, i.e. for a rather coarse grid. Even though the human eye can readily discern the positions of the holes in the right panel of figure 1 due to their regular arrangement, that is, essentially by detecting the common intersection between the three lines of peaks crossing at any site of the hexagonal lattice, an unconstrained automatic peak search for each maximum would lead in the present case to very ill-defined positions. We therefore chose to determine the smooth distortion vector field directly from the image of the hole pattern (after enhancement) as opposed to the above-mentioned two-step algorithm.

For the following discussion it is advisable to define the necessary concepts in mathematical terms: we specify the spatial distortions via the distortion vector field $f$, which maps a given point $x$ (in Cartesian coordinates) on the surface of the detector crystal to the two-dimensional signal $f(x)$. This means that $y = f(x)$ is the average detector response to a photon impinging at $x$, disregarding the stochastic noise in position determination. Due to the working principle of the detectors we can expect $f$ to be smooth, with the spatial frequency of the features being on the order of the distance between the photo-multiplier tubes. Note that for an ideal detector we have $f(x) = x$, corresponding to absolute fidelity in position determination. For undoing the effects of distortions we are interested in the inverse function $g$, so that $x = g(y)$ is the expected position on the detector crystal for a detector signal of $y$.

The positions of the peaks in the hole pattern image define the distortion vector field $y_i = f(x_i)$ evaluated at the regular positions of the holes of the mask $x_i$. We implemented the determination of the distortion vector field as a regularized minimization problem: define the

objective function

$$F(y_1, y_2, \ldots) = -\sum_i \int \mathrm{d}y E(y) K(y - y_i) + \lambda \sum_{\langle ij \rangle} V(y_i - y_j), \tag{1}$$

where $E$ is the image pattern after enhancement, $K$ is a Gaussian kernel with a width on the order of the width of the peaks in the pattern, $\lambda$ is a regularization parameter and $V$ is an energy functional with a minimum at the ideal nearest-neighbour distance (i.e. we imagine the peak positions as being connected by springs). $\langle ij \rangle$ denotes all pairs of nearest neighbours in the hexagonal lattice. The first sum quantifies the overlap between ideal peaks at $y_i$ and the image and therefore favours agreement between the positions $y_i$ and the (noisy) peak positions, whereas the second term punishes large deviations of the nearest-neighbour distances in the hexagonal lattice from their ideal values and therefore favours a smooth arrangement. The relative importance of these two effects is controlled by the regularization parameter $\lambda$. For those indices $i$ whose positions $y_i$ fall within a defined distance from the boundary of the illuminated region, the first term is ignored, leaving only the regularization constraint. Note that the integral in the first sum is actually implemented as a sum, too, because of the discrete nature of the pattern image, while the positions $y_i$ are treated as continuous variables.

It is advisable to solve this problem incrementally, which means to start with the central peak, find its optimal position and then iteratively add peaks on the boundary and relax the configuration according to equation (1). In this way, the inner peaks are already converged and the newly added peaks are therefore in the correct basin of attraction. Consequently, the algorithm hardly requires human guidance, only for some peaks outside of the illuminated region it can be beneficial to fix their position manually, so as to force an agreement on the very boundary due to the spring force. Starting with an ideal lattice and refining all positions at once, on the other hand, leads to the analogue of dislocations in the assignment of lattice sites to the maxima in the pattern image that anneal only very slowly, if at all. Once all the peak positions have preliminarily been assigned, one can vary $\lambda$ in order to either reproduce the small-scale position variations or rather have smooth modulations. The long-range modulations (on the order of the distance between the photo-multiplier tubes), however, are unaffected by a variation of $\lambda$ over a wide range. Also the position of the minimum in $V$ does not noticeably influence the determined peak positions within the illuminated region.

### *2.4. Distortion correction*

For a valid implementation of distortion correction one has to consider the discretization of the data: the image of a regular pixel grid under the correction function $g$ will in general not be regular. Therefore, especially for off-line algorithms, which correct whole images after the experiment, complicated approaches have been proposed which treat the shapes of the transformed pixels in various degrees of accuracy and re-distribute the counts to the pixels of a regular grid in proportion to the covered area (Spector *et al* 1972, Stanton *et al* 1992, Hammersley *et al* 1994). Note that such a direct redistribution of the counts inevitably leads to a smoothing and therefore destroys the Poissonian statistics of the original data. An implementation using the mathematically rigorous approach, where the counts are distributed stochastically according to a multinomial distribution, has not yet been reported. On-line algorithms, which treat each event on its own, in general obviate these issues either by correcting high-resolution signals before binning (Knoll and Schrader 1982, Johnson *et al* 1996) or

correcting the analogue signal (Muehllehner *et al* 1980). Note that an implementation where a digital input signal is deterministically mapped to an output signal of equal resolution and comparable amplitude produces moiré-like effects, as some output channels receive the counts from two input channels, whereas others stay empty (Knoll and Schrader 1982).

Due to the principle of ACPAR, for our purposes the data have to be treated on an event-by-event basis. Personal computers have nowadays reached storage capacities and computing powers, however, where it is possible to save the data in list mode to be evaluated afterwards, treating each event on its own. Our implementation was guided by the requirements to be efficient and modular, allowing for both on-line and off-line use and direct interfacing with the other stages of the evaluation pipeline.

The knowledge of the distorted positions $y_i = f(x_i)$ defines the inverse function $g$ on a distorted hexagonal grid. As our distortion data have a very fine resolution and are smooth due to the regularization, we define $g(y)$ for a general point $y$ by barycentric interpolation with respect to the corners of the triangle of the distorted hexagonal lattice in which $y$ lies. For efficiency we evaluate $g$ for each detector on the points of a $256 \times 256$ square lattice covering the whole area of the detector, and store the shifts to be applied as signed 16 bit integers in a look-up matrix.

Our detectors are read out with a resolution of 11 bits per dimension. As the magnitude of shifts to be applied is always below 30 channels, we use 8 bits of the look-up matrix for sub-channel accuracy. To avoid the above-mentioned moiré effect, we add a random sub-channel signal to our input values and truncate the output to the original resolution, which is the analogue to the concept of dithering in image processing. To be specific, our implementation

- reads the input signal in 11 bit resolution for each dimension,
- shifts the signal 21 bits to the left and fills the lower bits randomly,
- takes the 8 most significant bits as the indices into the look-up matrix,
- takes the 8 following bits as weighting factors for bi-linear interpolation,
- computes the interpolated displacement to be applied,
- adds the displacement (right-shifted by 3 bits to match the scale) to the input and
- right-shifts the result by 21 bits and truncates.

We implemented this distortion correction algorithm as a Unix filter acting on a byte stream, i.e. treating each event on its own. This allows us to easily set up an evaluation pipeline, optionally comprising custom masking filters, additional off-line energy discrimination or standard tools selecting only a subrange of events (such as `head`), and feeding the result into two-dimensional histogramming tools to produce either flood fields or ACPAR spectra. All the correction steps are implemented in 32 bit integer arithmetic and can therefore be very efficiently computed. For an off-line correction, the run-time is limited by the data transfer rate from the hard disk, being able to process about $2 \times 10^7$ positions per second, with a CPU load of about 30% on a contemporary personal computer. For an on-line evaluation, the load is negligible.

Any position correction of digitized signals necessarily introduces a blurring on the order of the channel width, as the input and output channel boundaries in general do not match. For detectors with inherent statistical noise such as Anger cameras, the detrimental effect is negligible, however, if the resolution of the sampling is sufficiently high. If the events are distributed to the output channels stochastically, as presented here, the statistical behaviour of the signal is not compromised, contrary to the standard algorithms for off-line position

correction as mentioned above. This means that the count values in the output pixels strictly follow Poissonian statistics and are therefore indistinguishable from a signal read out from an ideal detector, making it possible to, e.g., quantify the fit between experimental results and models by a $\chi^2$-test.

An additional benefit of the proposed implementation of distortion correction lies in the fact that the correspondence between the corrected position and the calibration pattern is by definition exact. Therefore the above-mentioned problem of calibrating the analogue amplification for each dimension of the signal for quantitative studies reduces to determining the lattice constant of the mask pattern and the distance between the mask and the source, both of which can be done with very high accuracy.

## 3. Discussion

### *3.1. Effects of distortion*

A characterization of the determined distortions and their effect on the homogeneity of illumination is illustrated in figure 2 for one of our detectors. Note that our goal here is to assess the merits of distortion correction and we therefore do not use a spatially varying 'sliding energy window' (Knoll and Schrader 1982) as an off-line energy discrimination step in addition to the detectors' built-in $511 \pm 35$ keV window. We begin our discussion with the original flood field. Three principal aspects can be discerned: even though the illumination in the central part of the detector looks comparatively homogeneous, the hexagonal arrangement of the photo-multiplier tubes has a small influence on the apparent illumination—directly over the centres of the tubes the count rate is higher; additionally, there are rather sharp rings with radius a little smaller than the distance between tubes around each tube. Secondly, the detector has an obvious flaw in the lower left quadrant, where illumination drops to around half of its mean value, which cannot be corrected by a re-calibration of the amplification of the pertaining photo-multipliers. Thirdly, the edge of the illuminated area shows significant deviations from the circular form of the lead aperture. The latter effect is obviously due to distortions, whereas at this point we cannot rule out the possibility that the two former effects are due to spatial variations in the energy signal amplification, although the fact that the flaw in the lower left quadrant is correlated to the deviations from the circular form in this region hints at a contribution of distortions also to this effect.

An inspection of the flood field after distortion correction shows that most of these effects disappear: the hexagonal pattern due to the arrangement of the photo-multiplier tubes has completely vanished, the above-mentioned flaw is largely repaired, and the edge of the illuminated region is nearly circular. We can therefore directly confirm that distortions are the major reason for flood field inhomogeneity, as was already indirectly concluded by Wicks and Blau (1979).

A direct quantification of the distortions is given in the lower part of figure 2 by an illustration of the vertical component of the shift vector field and its divergence, corresponding to integral and differential fidelity in position detection of the detector, respectively. The shift field has a very smooth appearance, and even in the divergence all observable features are directly due to effects of distortions that are also discernible in the uncorrected flood field. This reflects the fact that the effect of distortion correction is in first order just a normalization by the divergence, which has actually been used as an early approach for correcting the effects of distortion (Spector *et al* 1972). The sharp features at the boundary of the illuminated area are

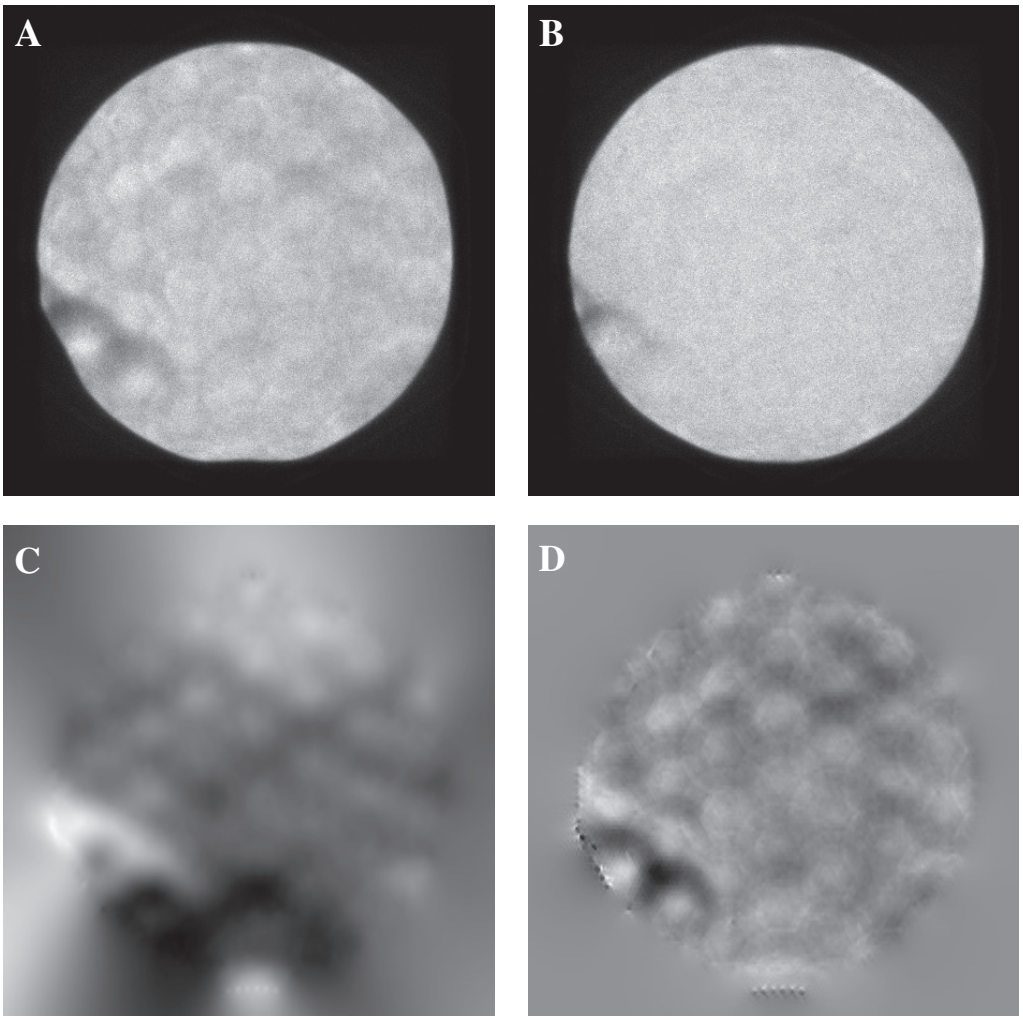


**Figure 2.** Obtained distortions and their effect. (A) Original flood field. (B) Flood field after distortion correction. (C) Vertical component of shifts to be applied; the variation in greyscale corresponds to a range of 35 channels (i.e. 2.3% of the detector diameter). (D) Divergence of the shift vector field; white and black correspond to area expansions and contractions of about 15%, respectively.

due to manual intervention in distortion determination as mentioned above, but, being outside of the illuminated area, these have no detrimental effects. Note that even though the displayed images have not been smoothed, there is virtually no noise discernible in the divergence. This demonstrates that due to the regularization the distortions can be determined very accurately even for our fine calibration pattern, which has been noted as a stringent condition for not introducing inhomogeneities into the corrected data by Muehllehner *et al* (1980) and Knoll and Schrader (1982).

### *3.2. Resolution gain in ACPAR spectra*

We judge the beneficial effect of distortion correction by its effect on two-dimensional ACPAR spectra. The essence of this method is to map the transverse momenta of the electrons in the sample by detecting the deviations from antiparallel propagation directions of pairs of photons

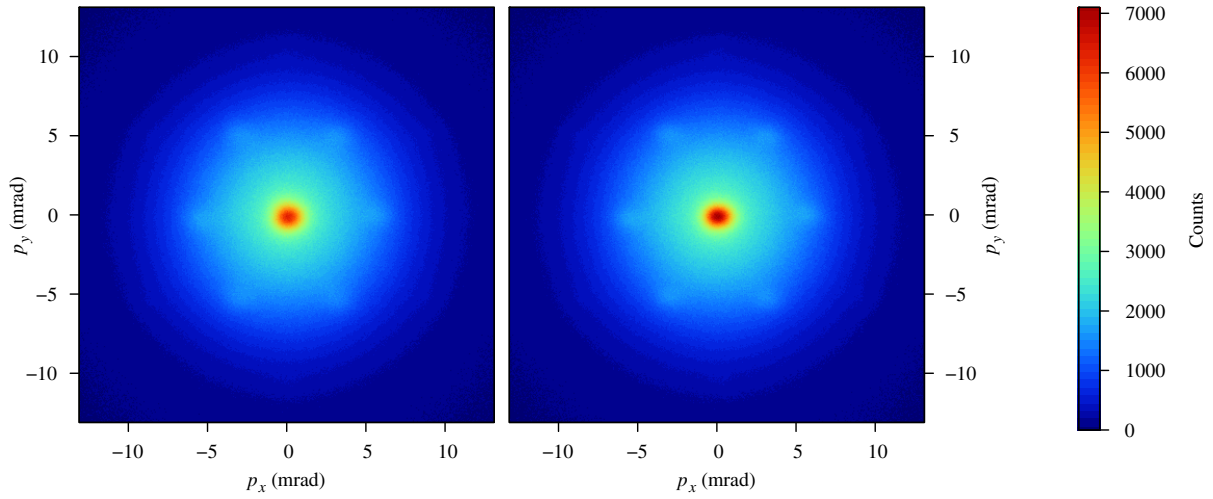


**Figure 3.** Two-dimensional ACPAR spectra computed from the same measurement before (left) and after distortion correction (right), rebinned to a channel size of $(0.066\,\text{mrad})^2$. Note that the pseudo-colour scale is common to both plots.

resulting from a single positron–electron annihilation event, which are linked due to momentum conservation. Here the limiting factor for the achievable resolution is the position assignment of the photons. The effect of inhomogeneous illuminations, on the other hand, can be easily corrected. The detrimental effect of systematic distortions due to the regular arrangement of the detector tubes in Anger cameras has already been recognized (West 1995), and it has been proposed to rotate the detector tube lattices with respect to each other, so that the distortions only lead to an isotropic resolution loss as opposed to introducing artificial features into the spectra.

An ACPAR experiment on single crystalline quartz constitutes the most sensitive test of resolution: it is known that apart from the majority of positrons that annihilate with bound electrons and give a broad background in the spectra, a minority of positrons capture an electron and form a positronium state that is delocalized over the crystal. The self-annihilation of these states yields peaks at the reciprocal lattice positions with a width that is ideally given only by the thermal Boltzmann distribution of the delocalized positronium atoms (Brandt *et al* 1969). Experimentally, the peak width is additionally broadened by the instrumental resolution, composed of the uncertainty of the position at the detector (which, in general, is isotropic) and the position of annihilation (which is significant only in the horizontal direction because of the limited penetration length of the incident positron beam).

Figure 3 shows the two-dimensional spectra of a quartz single crystal, oriented with its sixfold axis along the projection direction, both with and without distortion correction. In both cases the sixfold symmetry with the first higher-order momentum components of delocalized positronium, which are slightly better defined after distortion correction, is clearly visible; also the second-order components show a faint signature. The most obvious difference is in the central peak, however: as the same total number of counts is plotted with the same pseudo-colour scale, the higher peak intensity after distortion correction directly shows the gain in resolution. Furthermore, after distortion correction the resolution anisotropy due to the beam spot size is clearly visible.

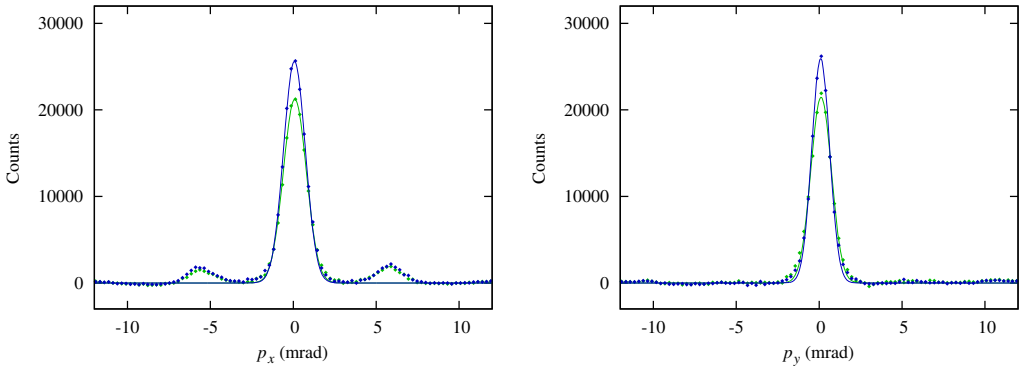


**Figure 4.** Cut through the central peak after subtraction of the fitted background: horizontal (left) and vertical cut (right), before (green) and after distortion correction (blue). Points are data and lines are fits. The satellite peaks in the horizontal cut are the higher-order components at the first reciprocal lattice position of the hexagonal quartz lattice at 5.70 mrad.

For a quantitative evaluation we observe that the broad component can be well fitted by an isotropic Gaussian with $\sigma = 4.9$ mrad, both before and after distortion correction. Cuts through the central positronium peak, after subtracting this fitted background, are presented in figure 4. It can be seen that the peak form (and therefore the resolution function) can be well described by a Gaussian in the central parts, whereas the outer regions show leptokurtic behaviour. This is in agreement with earlier findings (Kruseman 1999). We therefore fitted two-dimensional Gaussians to the data, using the fitted function itself as the weighting factor (determined self-consistently). The figure shows that with this approach the central parts of the peaks can be described very satisfactorily. The resulting widths are $\sigma^{\mathrm{h}} = 0.622(1)$ mrad and $\sigma^{\mathrm{v}} = 0.695(1)$ mrad without distortion correction, and $\sigma_{\mathrm{c}}^{\mathrm{h}} = 0.538(1)$ mrad and $\sigma_{\mathrm{c}}^{\mathrm{v}} = 0.655(1)$ mrad after distortion correction, respectively, corresponding to a mean contribution of the distortions to the point spread function of 0.26 mrad or equivalently 2.2 mm.

The resulting resolution anisotropy is 0.374(3) mrad. It corresponds to a beam width of 1.54(1) mm (standard deviation), which is in agreement with direct measurements (Ceeh *et al* 2012).

The calibration pattern image can also be used for quantifying the statistical noise in the position assignment: for this purpose, we subject the original calibration image to the distortion correction algorithm and compute its two-dimensional auto-correlation function. This auto-correlation function shows again the hexagonal pattern that quantifies the overlap between the lattice and its shifted copy for general shift vectors. The modulation of this pattern does not decay even for large shift vectors, which proves that no 'lattice defects' have been built in during the distortion calibration step. The relative amplitude of the modulation is only $1.22 \times 10^{-4}$, reflecting the fact that also the modulation in the calibration images is rather faint. The statistical accuracy of the modulation in the auto-correlation is very high, however, as it quantifies essentially the overlap of every pair of peaks. Reproducing this value by computing the auto-correlation of a model hexagonal pattern with the known geometry smeared by a Gaussian function gives a standard deviation of 1.64 mm for the statistical point spread function. This is in satisfactory agreement with the value of 1.9 mm obtained from a determination of the sharpness of an illuminated edge, and the value reported by the detector

manufacturer of 3.5 mm (full-width at half-maximum). A comparison of these values with the reduction of the point spread function of 2.2 mm effected by distortion correction shows that distortion correction results in an increase of the detector resolution by a factor of 1.7.

The discrepancy between the residual instrumental point spread function of about 0.20 mrad and the measured width is due to thermal excitation of the annihilating positronium atoms. Its high value reflects the fact that the effective band mass of positronium in quartz is much larger than the actual mass of $2m_e$ (Ikari and Fujiwara 1979).

### *3.3. Temporal stability*

A critical issue left to treat is the temporal stability of the determined distortions. After all, the benefit of the reported gain in detector resolution is limited if it comes at the price of having to allocate a significant amount of measurement time to taking test patterns for recalibration. In fact, Heiderich *et al* (1991) have reported the necessity for daily readjustments of the photo-multiplier parameters in an Anger-type camera; in contrast, Muehllehner *et al* (1980) report no significant variation during six months of operation. This is consistent with our experience: for ACPAR studies it is necessary to measure, apart from the actual data taken in coincidence mode, also flood fields, which means frames without a coincidence criterion (the so-called singles spectra), for each detector, in order to correct for possible illumination gradients over the detectors due to different sample absorptions for different photon directions. If such effects are visible at all, they are very smooth due to the fact that a detector covers only a very small solid angle. As we have demonstrated above that spatial distortions leave characteristic small-scale modulations in the flood fields, a visual inspection of these singles spectra with regard to small-scale inhomogeneities can serve as a criterion to judge the necessity for recalibration. In our case, the distortion correction look-up matrix has proven to stay accurate during several months of operation, as long as one does not change the individual photo-multiplier amplifications.

## 4. Conclusion

We have presented a direct determination of the spatial distortions inherent to any detector of Anger type, and we have shown that most of the systematic deviations from an ideal performance are due to distortions. We proposed an efficient implementation of a correction algorithm processing each event in turn, and we demonstrated the resulting significant improvement of detector resolution by a factor of 1.7 in two-dimensional ACPAR measurements. The proposed algorithms are independent of the type of detector or whether some algorithm for distortion correction is implemented in hardware and can therefore be used to improve the performance of any existing spectrometer without much effort. As the inhomogeneities of a flood field illumination have been demonstrated to be primarily due to distortions, the potential gain or the need for subsequent re-calibration due to temporal drifts in the components can be judged from the flood field appearance.

## Acknowledgments

This work was supported by the Deutsche Forschungsgemeinschaft via the Transregional Collaborative Research Center TRR 80 ‘From Electronic Correlations to Functionality’.

## References


Anger H O 1958 *Rev. Sci. Instrum.* **29** 27–33

Barendt S, Modersitzki J and Fischer B 2007 *'Bildverarbeitung für die Medizin 2007' Informatik aktuell* ed A Horsch, T M Deserno, H Handels, H-P Meinzer and T Tolxdorff (Berlin: Springer) pp 449–53

Brandt W, Coussot G and Paulin R 1969 *Phys. Rev. Lett.* **23** 522–4

Ceeh H, Weber J A, Leitner M, Böni P and Hugenschmidt C 2012 Performance of the new 2D ACAR spectrometer in Munich *Rev. Sci. Instrum.* submitted (arXiv:1210.3497 [physics.ins-det])

Coates L, Stoica A D, Hoffmann C, Richards J and Cooper R 2010 *J. Appl. Cryst.* **43** 570–7

Engeland U 2001 Untersuchungen zur Optimierung eines Gammakameradetektors durch die Auswertung seiner verrauschten Antwort auf die Gammaquanten aus einer verfahrbaren Feinnadelstrahlquelle *PhD Thesis* Universität Göttingen

Engels R, Clemens U, Kemmerling G, Nöldgen H and Schelten J 2009 *Nucl. Instrum. Methods* A **604** 147–9

Hammersley A P, Svensson S O and Thompson A 1994 *Nucl. Instrum. Methods* A **346** 312–21

Heiderich M, Reinartz R, Kurz R and Schelten J 1991 *Nucl. Instrum. Methods* A **305** 423–32

Ikari H and Fujiwara K 1979 *J. Phys. Soc. Japan* **46** 92–6

Johnson T K, Nelson C and Kirch D L 1996 *Phys. Med. Biol.* **41** 2179

Knoll G F and Schrader M E 1982 *IEEE Trans. Nucl. Sci.* **29** 1271–9

Kruseman A C 1999 Two-dimensional ACAR and low-background DBAR studies on materials with defects *PhD Thesis* Delft University of Technology

Muehllehner G, Colsher J G and Stoub E W 1980 *J. Nucl. Med.* **21** 771–6

Parmar A N, Martin D D E, Bavdaz M, Favata F, Kuulkers E, Vacanti G, Lammers U, Peacock A and Taylor B G 1997 *Astron. Astrophys. Suppl. Ser.* **122** 309–26

Schultz A J, Lurgio P M D, Hammonds J P, Mikkelson D J, Mikkelson R L, Miller M E, Naday I, Peterson P F, Porter R R and Worlton T G 2006 *Physica* B **385–6** 1059–61

Short M D 1984 *Nucl. Instrum. Methods* **221** 142–9

Spector S S, Brookeman V A, Kylstra C D and Diaz N J 1972 *J. Nucl. Med.* **13** 307–12

Stanton M, Phillips W C, Li Y and Kalata K 1992 *J. Appl. Crystallogr.* **25** 549–58

West R N 1995 *Positron Spectroscopy of Solids* ed A Dupasquier and A P Mills Jr (Amsterdam: IOS Press) pp 75–143

West R N, Mayers J and Walters P A 1981 *J. Phys. E: Sci. Instrum.* **14** 478

Wicks R and Blau M 1979 *J. Nucl. Med.* **20** 252–4

Zanzonico P and Heller S 2007 *Clinical Nuclear Medicine* ed H-J Biersack and L M Freeman (Berlin: Springer) pp 1–33